Research Article

Xiaoxiao Wang, Dexi Li, Ru Bai*, Shuguang Liu, Changwang Yan, and Ju Zhang

Evolution of the pore structure of pumice aggregate concrete and the effect on compressive strength

https://doi.org/10.1515/rams-2023-0112 received April 01, 2023; accepted July 26, 2023

Abstract: China possesses abundant pumice resources and thereby makes the utilization of pumice in the preparation of pumice aggregate concrete (PAC) a significant strategy for environmental protection and resource conservation. To obtain the effect of pumice pore structure variation on the compressive strength of PAC, PACs with strength classes LC20, LC30, and LC40 were prepared. Moreover, the pore structure of PAC was characterized using nuclear magnetic resonance to investigate the effect of pore structure variation on the compressive strength of PAC. Results showed that the higher the coarse aggregate content of PAC, the higher the percentage of large capillary and non-capillary pore sizes of PAC, corresponding to higher porosity and lower compressive strength. The hydration products in PAC continuously fill in the pore structure, the proportion of large capillary pores and non-capillary pore size gradually decreases, the proportion of small capillary pores and medium capillary pore size gradually increases, the pumice concrete matrix gradually becomes dense, and the compressive strength increases. The prediction model of the pore structure and compressive strength is established based on gray theory, and the relative error between predicted and tested values is not significant,

which can effectively predict its compressive strength. It provides effective guidance for the engineering practical application of PAC.

Keywords: pumice aggregate concrete, pore structure, compressive strength

1 Introduction

Concrete is composed of cement, water, aggregates, and various additives and is one of the most commonly used construction materials in the world due to its durability and high plasticity. Among the components of concrete, aggregates play a crucial role, constituting approximately 60-80% of the total volume of concrete [1]. With the construction industry witnessing substantial growth, the demand for aggregates has surged significantly, leading to a scarcity of natural sand and gravel resources. To mitigate the consumption of these finite resources, alternative options such as natural lightweight rocks are employed as coarse aggregates in concrete production. Examples of such lightweight rocks include expanded perlite [2], slate [3], coral stone [4], and pumice [5]. Pumice, in particular, stands out due to its easy availability, convenient construction process, lower cost, and outstanding properties [6]. Utilizing pumice as an aggregate for concrete preparation can effectively curtail the depletion of natural sand and gravel resources.

Pumice, also referred to as light stone, is a widespread natural material with a rough texture. It is found abundantly across the globe, with Italy being the largest producer and China, Spain, Greece, and Turkey possessing substantial reserves [7]. Lightweight concrete, utilizing highly porous pumice as a coarse aggregate, exhibits commendable thermal insulation [8], freeze—thaw resistance [9,10], and seismic performance [11]. As the most fundamental characteristic of concrete, mechanical properties have been the subject of extensive research concerning pumice aggregate concrete (PAC). For instance, Kashyap

^{*} Corresponding author: Ru Bai, School of Materials Science and Engineering, Inner Mongolia University of Technology, Hohhot 010051, China, e-mail: 20201000035@imut.edu.cn

Xiaoxiao Wang: School of Civil Engineering, Inner Mongolia University of Technology, Hohhot 010051, China; Key Laboratory of Civil Engineering Structure and Mechanics, Inner Mongolia University of Technology, Hohhot 010051, China; Inner Mongolia Engineering Research Center of Ecological Building Materials and Prefabricated Construction, Hohhot 010051, China

Dexi Li, Ju Zhang: School of Civil Engineering, Inner Mongolia University of Technology, Hohhot 010051, China

Shuguang Liu, Changwang Yan: School of Materials Science and Engineering, Inner Mongolia University of Technology, Hohhot 010051, China; School of Mining and Technology, Inner Mongolia University of Technology, Hohhot 010051, China

and Sasikala [12] replaced natural coarse aggregates with pumice aggregates at various replacement rates (0, 10, 20, 30, and 40%) to produce concrete. Comparing the results with ordinary concrete, it was observed that the concrete's porosity gradually increased with higher replacement rates, leading to a reduction in compressive strength by 9, 14, 18, and 21%. Despite this, the compressive strength remained higher than the values specified in the standard. Similarly, Liu et al. [13] manufactured ultra-high performance concrete (UHPC) by replacing river sand with pumice aggregate. The study revealed that pumice aggregate possessed a high porosity ranging from 51.6 to 56%, a pore connectivity of 99.8%, and an average pore size of 5.8 µm. Additionally, the pore-rich structure of pumice aggregate contributed to the reduction of self-shrinkage in UHPC without compromising its mechanical properties. From this, it can be observed that different scholars have obtained diverse trends regarding the compressive strength of concrete incorporating pumice aggregates. Therefore, investigating the influence of pumice aggregates on concrete's compressive strength is crucial to optimize their usage in concrete preparation.

PAC is considerably known to be a typical porous material. Moreover, the pore structure within concrete is an inherent physical property, with the microstructure playing an important role in influencing macroscopic mechanical properties and durability [14], focusing mainly on qualitatively exploring the influence of pore structure characteristics and interface structure on performance. In response to the inadequate quantitative research, Erenson and Kalkan [15] assessed the PAC compressive strength and porosity correlation by digital image processing to determine the relationship between the pore structure and macroscopic properties. Liu et al. [16] obtained the freezing law of interstitial water of pumice concrete using the nuclear magnetic resonance (NMR) technique, studied the effect of pore water freezing on the compressive strength of pumice concrete under a low-temperature environment, and found that the increase of compressive strength is caused by the freezing of interstitial water of 0.1-1 µm, and finally, established the compressive strength model considering the freezing stress. Gao et al. [17] used a combination of gray correlation and multiple linear regression analysis to explore the relationship between the mortar pore size and macroscopic properties and established a multiple linear regression equation. Nasharuddin et al. [18] tested the pore size distribution of cemented paste backfill materials using NMR spectroscopy. Accordingly, they described the effect of pore size distribution on macroscopic properties and established the relevant equations. Santos et al. [19] tested the pore structure of mortars and evaluated the effect of pore size distribution on compressive strength, establishing a link between the two aspects. Liu *et al.* [20] investigated the microstructural characteristics of light-aggregate concrete with wind-deposited sand using the NMR spectroscopy. Moreover, they applied gray theory to explore the relationship between the fractal dimensions of 0–0.1, 0.1–10, and >10 μ m and compressive strength; and established a GM(1,4) gray model for predicting the compressive strength. In summary, it can be found that there is a huge link between the microscopic pore structure and the macroscopic properties of concrete, and minimal research has been conducted on the macroscopic performance of the pore structure evolution law of PAC. Furthermore, the pore relationship, based to find the strength prediction model of PAC, is yet to be established.

In this study, we prepared PAC with pumice as coarse aggregate, and the pore structure parameters of PAC with different strengths were measured using NMR spectroscopy to analyze changes in porosity, pore size distribution, and fractal dimension. The objective is to reveal the evolutionary pattern of the pore space of the pumice aggregate during the maintenance period on the changing pattern of the compressive strength. Finally, the compressive strength prediction model of PAC was established by analyzing the magnitude of the influence of the hole parameters on the macroscopic properties by means of Dunn's correlation.

2 Materials and test methods

2.1 Test materials and matching ratio

Cement is P.O 42.5 ordinary silicate cement. Coarse aggregate is pumice aggregate with particle sizes between 5 and 20 mm in Inner Mongolia. Figure 1 shows the morphological characteristics of natural pumice. Note that the



Figure 1: Morphological characteristics of pumice aggregate.

Table 1: Physical properties of pumice aggregate

Physical properties	Bulk density (kg·m ⁻³)	Apparent density (kg·m ⁻³)	Water absorption (%)	Uniaxial compressive strength (MPa)	Loss on ignition (%)	Acid insoluble (%)
Test value	810	1690	17.6	2.77	3.31	76.63

Table 2: Chemical properties of pumice aggregate

Chemical composition	SiO ₂	Al ₂ O ₃	Fe ₂ O ₃	CaO	MgO	Na ₂ O	Other
Content (%)	45.62	15.26	10.46	8.37	6.96	5.24	8.09

surface of pumice aggregate is considerably rough, mainly with open pores, irregular pore shape, and uneven pore size distribution. The main physical properties of pumice aggregates are shown in Table 1 and the chemical properties are shown in Table 2. Table 2 shows that the SiO2 and Al₂O₃ contents of the pumice aggregate are high, and studies have shown that pumice aggregate has volcanic ash activity [21]. The fine aggregate is ordinary river sand with a coarseness of medium sand and a moisture content of 2.31%, apparent density of 2,550 kg·m⁻³, and bulk density of 1,590 kg m⁻³. Fly ash is produced at the Huaneng Diangiao Thermal Power Plant in Hohhot. The water-reducing agent is the naphthalene ordinary water-reducing agent and dosing of 1% of the cementitious material. The water used is municipal tap water.

Combined with years of research on PAC by Wang et al. [22], as well as a large number of experimental practices, the PAC proportions in this study were determined. They not only can meet the construction requirements of the actual project but also ensure the compatibility of the concrete preparation. The specific PAC mix is shown in Table 3, and the specific characteristics of natural pumice concrete are shown in Table 4.

It is worth noting that, due to the low density of pumice aggregate, surface porosity, and other characteristics, the pumice aggregate was placed in water to soak and absorb water for 12 h before preparing PAC to ensure that the pumice aggregate reaches a saturated state, which increases the quality of pumice aggregate after treatment, reduces the water absorption of pumice aggregate, and avoids the phenomenon of pumice aggregate floating. Then, the pumice aggregate was face-dried before the concrete mix was mixed, and the water absorbed by the pumice aggregate was added to the mix to avoid the water/cement ratio being affected by the water absorbed by the aggregate during the preparation of PAC and to ensure that the fluidity of the mix was not affected.

2.2 Test methods

2.2.1 NMR spectroscopy test

The T_2 spectrum measured using NMR spectroscopy is well known to be able to reflect the environment of hydrogen

Table 3: Mix proportion of PAC

Sample	Water (kg)	Cement (kg)	Fly ash (kg)	Sand (kg)	Pumice (kg)	Water reducer (kg)	Water/glue ratio	Sand rate (%)
LC20	150	300	75	841	588	3.75	0.4	42
LC30	144	320	80	739	562	4	0.36	40
LC40	136	340	85	644	532	4.75	0.32	38

Table 4: Properties of PAC

Sample	Strength of 28 days (MPa)	Water/blinder ratio	Split tensile strength (MPa)	Elastic modulus (10 ⁴ MPa)	Poisson's ratio	Slump (cm)	Dry density (kg·m ⁻³)
LC20	24.92	0.46	0.97	2.37	0.14	0.21	1891.73
LC30	32.02	0.33	1.52	2.60	0.17	0.18	1943.73
LC40	33.71	0.30	1.80	2.96	0.18	0.17	1948.30

protons in the specimen, and that the hydrogen protons inside the concrete are subject to binding forces. That is, it is the binding force generated by the pore structure in the specimen, so the pore characteristic parameters of the specimen can be obtained by further analysis of the T_2 spectrum measured by NMR spectroscopy [23]. The relationship between the relaxation time T_2 and the pore size r can be expressed as [24]

$$\frac{1}{T_2} = \rho_2 \left(\frac{S}{V} \right)_{\text{pore}} = \rho_2 \left(\frac{F_s}{R} \right), \tag{1}$$

where T_2 is the transverse relaxation time, ms; S is the pore surface area, μm^2 ; V is the pore fluid volume, μm^3 ; ρ_2 is the transverse relaxation rate, $\mu m \cdot m s^{-1}$; F_s is the pore shape factor, which is 3 for spherical and 2 for columnar [25]; and R is the pore radius, μm .

For the same specimen, the surface relaxation strength ρ_2 and the pore shape factor F_s are constant. By defining $\rho_2 \cdot F_s$ as a constant N, and continuing to take the logarithm of Eq. (1), we have



Figure 2: NMR test equipment.

$$\lg T_2 - \lg N = \lg R. \tag{2}$$

After comparing the cumulative NMR T_2 distribution curves with the cumulative distribution curves of the mercury–pressure aperture, the curve that best matched the two measurements was used to calculate the N value [26]. The N value is returned to the T_2 spectrum measured by NMR spectroscopy, which is able to complete the conversion from the T_2 spectrum to the pore size; signal amplitude corresponds to the pore volume. The N values of pumice aggregate and PAC are 0.1 and 3, respectively.

Specimens with a height of 50 mm and a diameter of 50 mm were prepared for NMR testing of pumice aggregate and PAC. The Shanghai Newmark MesoMR-60S NMR instrument was used, and the test conditions were as follows: instrument magnetic field strength, 0.5 ± 0.08 T; main frequency, 21.3 MHz; echo number, 2,048, 64 scans; and NMR test instrument (Figure 2).

The NMR test procedure is shown in Figure 3. When the NMR specimens reach the specified curing age (7, 14, 21, and 28 days) in the standard curing environment (temperature, $20 \pm 2^{\circ}$ C; relative humidity, $95 \pm 5\%$), the specimens were put into the vacuum saturator 1 day in advance for the vacuum saturation treatment of the specimens with a vacuum pressure value of 0.1 MPa for 24 h. After completion of saturation, the specimens were wrapped underwater with a waterproof tape and placed in an NMR test apparatus to carry out NMR experiments to obtain porosity and the T_2 spectra of PAC at each curing age. After the completion of each age test, the specimens were returned to the standard maintenance environment for further maintenance and the completion of subsequent age tests.

2.2.2 Compressive strength test

The PAC specimens were prepared to a size of 100 mm \times 100 mm \times 100 mm according to test standards. Then, standard conservation (temperature, 20 \pm 2°C, relative humidity, 95 \pm 5%) and compressive strength testing were performed after reaching the curing age (*i.e.*, 7, 14, 21, and 28 days). According to the Standard for Mechanical Properties

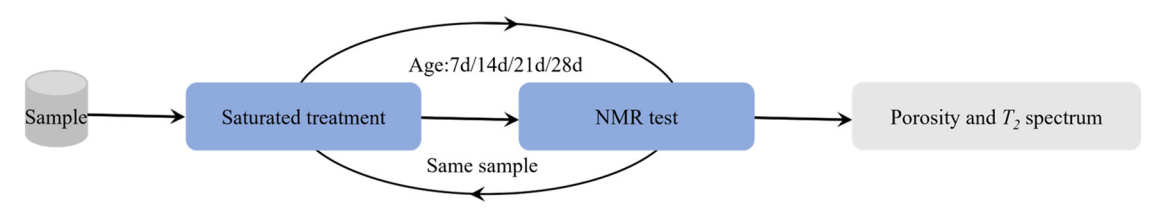


Figure 3: Flow chart of NMR.

Test Methods of Common Concrete (GB/T50081-2002), the YAS-600 microcomputer-controlled electro-hydraulic servo high stiffness rock uniaxial pressure tester manufactured by Changchun Xinte was used to test the PAC. The loading rate was 0.5 MPa·s⁻¹. The test equipment is shown in Figure 4.

3 Results and analysis

DE GRUYTER

3.1 Pore structure characteristics of pumice aggregate

Four types of pores were classified according to Kumar and Bhattacharjee [27]: small capillaries (0-0.1 µm), medium capillaries (0.1-1 µm), large capillaries (1-10 µm), and noncapillaries (>10 µm). According to the NMR test, it is known that the porosity of pumice aggregate ranges from 17.92 to 45.73%, that of expanded clay ranges from 39.28 to 48.39%, and that of expanded slate [28] ranges from 29.60 to 37.96%. It can be found that pumice has similar porosity to expanded clay and expanded slate, and the pore structures are richer. In this study, we classified pumice aggregate into classes I and II based on their pore size distribution characteristics. Two typical pumice aggregate pore size distributions are shown in Figure 5. Note that both pumice pore sizes are distributed between 1 and 100,000 µm. The pore size distribution graph of the class I pumice aggregate shows two peaks. The main peak is distributed around 10,000 µm, which belongs to non-capillary pores and is the main pore

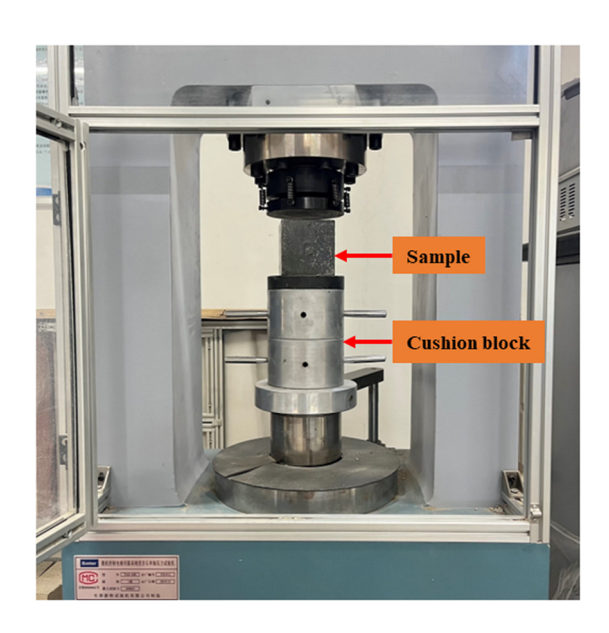


Figure 4: Compressive strength test piece and test equipment.

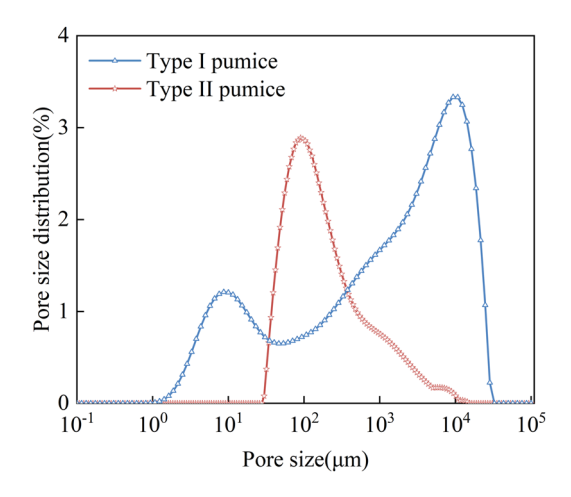


Figure 5: Pore size distribution of pumice aggregate of types I and II.

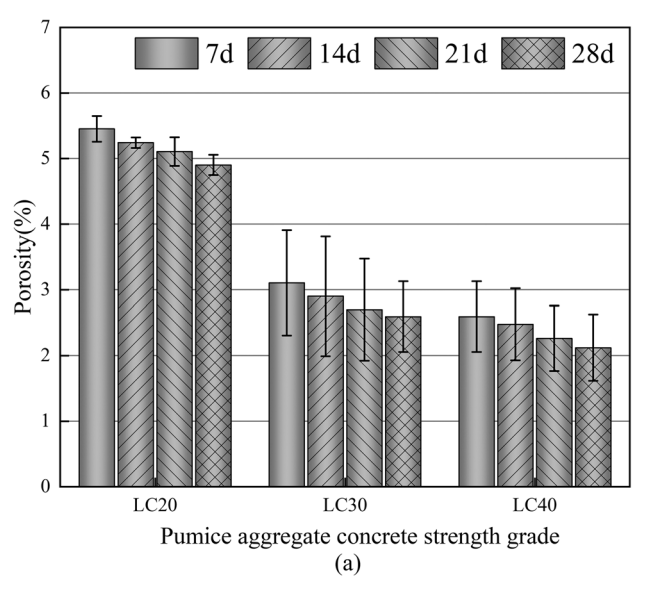
size distribution interval of pumice. The secondary peak appears around 10 µm, which indicates that the pumice aggregate also has some large capillary pores inside, accounting for a relatively small percentage. The pore size distribution diagram of class II pumice aggregate shows only one wave peak, located around 100 µm, and has a smaller pore size span and more uniform pore size compared with the class I pumice. In this study, we selected the pumice aggregate mixes of classes I and II to prepare PAC. Thus, the pore size distribution of the pumice aggregate mixes showed three wave peaks.

3.2 Pore structure evolution law of PAC

3.2.1 Porosity

The variation pattern of the porosity of PAC under different curing ages is shown in Figure 6. As shown in Figure 6(a), the porosities of LC20, LC30, and LC40 show a decreasing trend with an increase in curing age. For example, the porosity of LC20 PAC was 5.46% at a curing age of 7 days, which decreased to 4.91% when it reached 28 days; this resulted in a decrease of 10.07% compared with the porosity percentage at 7 days. LC30 and LC40 showed the same pattern, with the porosity percentages at 28 days decreasing by 21.51 and 17.69%, respectively, compared with the porosity percentage at 7 days. Although the porosity of expanded perlite concrete [29] ranged from 15.1 to 48.3%, PAC had lower porosity compared to that of expanded perlite concrete. The reduction in the porosity of PAC is caused by two factors.

1) Reduction in porosity of coarse and fine aggregate accumulation: During the maintenance process, cement undergoes hydration reactions and the resulting hydration 6 — Xiaoxiao Wang et al. DE GRUYTER



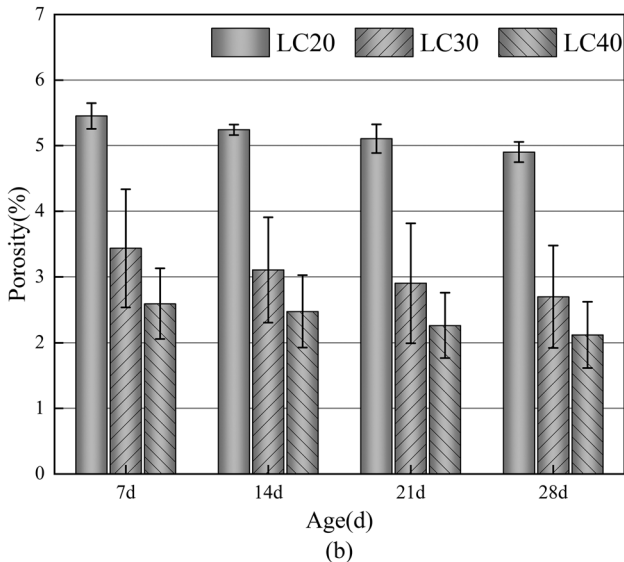


Figure 6: Porosity of PAC: (a) different strengths and (b) different curing ages.

products fill the pores due to the accumulation of coarse and fine aggregates [30].

2) Reduction of pumice aggregate's own porosity: In PAC, the porosity of pumice aggregate is between 17.92 and 45.73%, and its pore size is mainly distributed in the range of non-capillary pores. Accordingly, hydration products may fill the pores of the pumice aggregate itself, thereby leading to a reduction in porosity.

The combined effect of the two aspects causes the decrease in the porosity of PAC with increasing age of curing.

Figure 6(b) shows that LC20 has the highest porosity at the same age, followed by LC30, with LC40 having the lowest porosity. Since the coarse and fine aggregate content of LC20 is the highest, the resulting aggregate pile porosity and the pumice aggregate provide a larger porosity. Another reason is that as the cement content of PAC is different under varying strength levels, the content of hydration products produced by cement increases with strength level, and the corresponding porosity filled by hydration products will also increase.

3.2.2 Pore size distribution

Figure 7(a) shows the pore size distribution of LC20 PAC, indicating a bimodal pattern. Most of the pore size of Peak1 is 0.38 μ m, which is in the range of medium capillary pores, and the Peak1 aperture accounts for about 25%. Most of the pore size of Peak2 is 16.59 μ m, which is in the range of non-

capillary pores, and the Peak2 aperture accounts for about 15%. Figure 7(b) and (c) shows the pore size distribution plots of LC30 and LC40 PAC, respectively. Compared with LC20, the pore size distribution plots of LC30 and LC40 show a three-peak pattern. Among them, the most available pore size of Peak1 remains unchanged at 0.38 µm, but the percentage of its corresponding pore size increases to 35 and 47%. Moreover, the peak heights of Peak1 of LC30 and LC40 gradually increased with an increase in the intensity level, and the peak heights of Peak2 and Peak3 showed an opposite pattern. The pore size distribution map of PAC at the same strength level also changed. Considering LC30 as an example, the pore size percentage of Peak2 increased from 13.21 at 7 days to 17.49% at 28 days, and the pore size percentage of Peak3 decreased from 16.71 at 7 days to 12.95% at 28 days. The pore size percentage changes of Peak2 and Peak3 may be influenced by cement hydration. That is, as the age of maintenance increases, hydration intensifies and the resulting hydration products gradually fill in the pores of the aggregate pile and fill within the pores of the pumice aggregates itself. The filling of hydration products leads to the gradual differentiation of non-capillary pores (pore size >100 μm) in PAC into large capillary pores (pore sizes in the range of 1–10 µm). Among them, coral concrete [31] has about 16% of the most available pore size of small capillaries and 5% of the most available pore size of medium capillaries, and PAC has a larger percentage of small and medium capillaries compared to coral concrete; moreover, PAC is more abundant in small pores, while both have the same three-peak distribution.

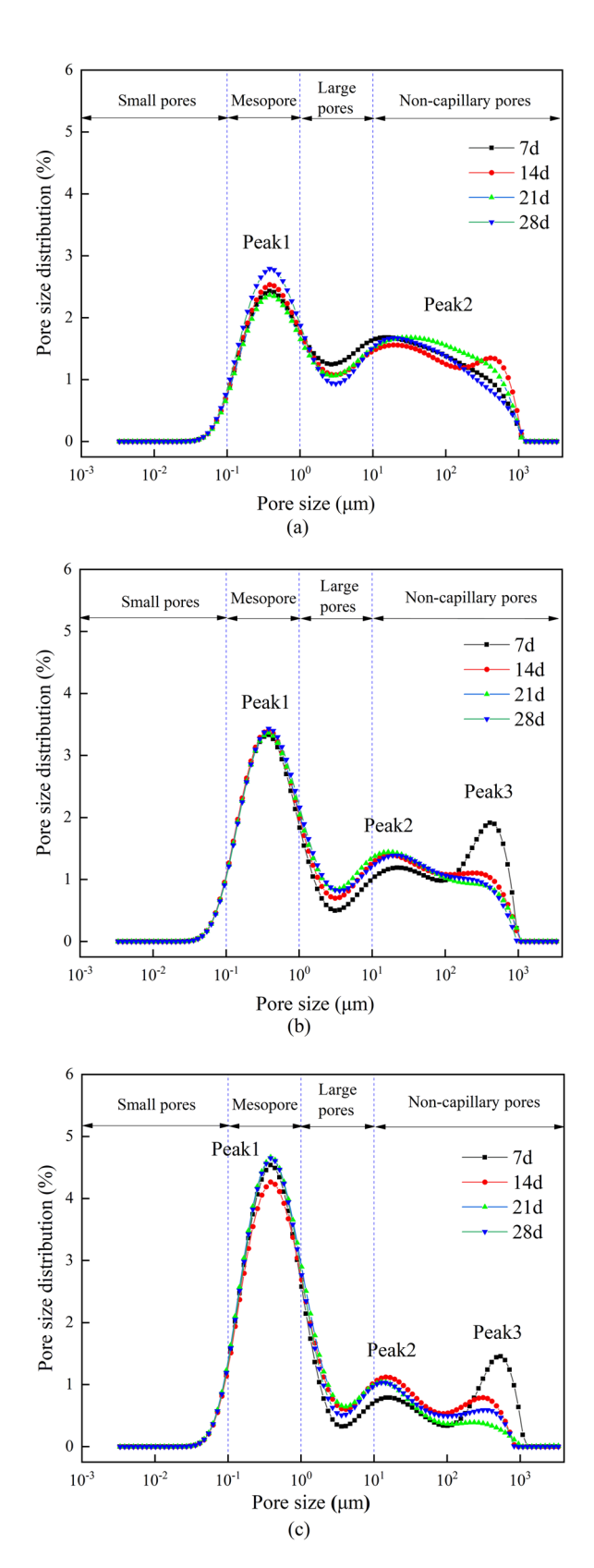


Figure 7: Pore size distribution of PAC: (a) LC20, (b) LC30, and (c) LC40.

3.3 Compressive strength of PAC

Figure 8 shows the changes in the compressive strength of PAC at different curing ages. It can be seen that the compressive strength of LC20, LC30, and LC40 show an increasing trend with the growth of the age of maintenance. For example, the compressive strength of LC20 PAC is 17.78 MPa at the curing age of 7 days and increases to 24.92 MPa when it reaches 28 days, which is an increase of 7.14 MPa compared with that at 7 days. The compressive strengths of LC30 and LC40 showed the same pattern, and the compressive strengths at 28 days increased by 8.64 and 8.72 MPa, respectively, compared with those at 7 days. This is due to the filling of the pumice aggregate porosity and pore size by the hydration products and the gradual increase in the compressive strength of the PAC. From the above, it can be seen that the porosities of LC20, LC30, and LC40 decreased by 0.55, 0.74, and 0.46%, respectively, compared to those at 7 days, and 0.46%, respectively. In addition, the percentages of Peak1 and Peak2 pore size increased, non-capillary pores gradually differentiated into large and medium capillary pores, and the matrix gradually compacted, resulting in the compressive strength of PAC increasing with an increase in curing age.

3.4 Mechanism of the effect of pore structure of pumice aggregate on the compressive strength of PAC

The fractal dimension of concrete can be used to characterize the complexity of the spatial distribution morphology of the cement matrix pores; that is, the larger the fractal dimension of the pore volume, the more complex the spatial distribution morphology of the pores and the greater their space-filling capacity [32]. In this study, we obtained the fractal dimension of the pore volume of PAC using the NMR method [33], in which the fractal geometry of the geometric fractal principle [34] is formulated as follows:

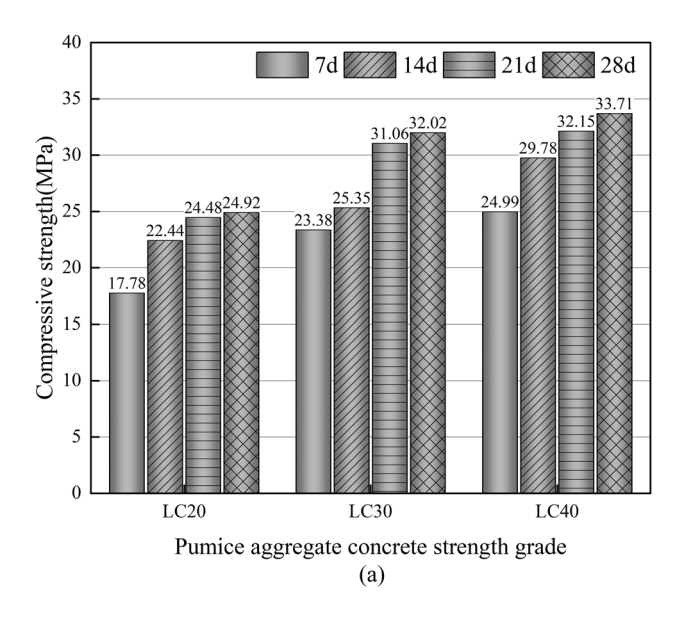
$$S_{v} = \left(\frac{T_{2 \text{ max}}}{T_{2}}\right)^{D-3}.$$
 (3)

Further simplification gives

$$\log S_{\rm v} = (3 - D)\log T_2 + (D - 3)\log T_{\rm 2 max},\tag{4}$$

where T_2 exhibits a proportional conversion relationship with the pore radius. Eq. (4) is further converted as follows:

8 — Xiaoxiao Wang et al. DE GRUYTER



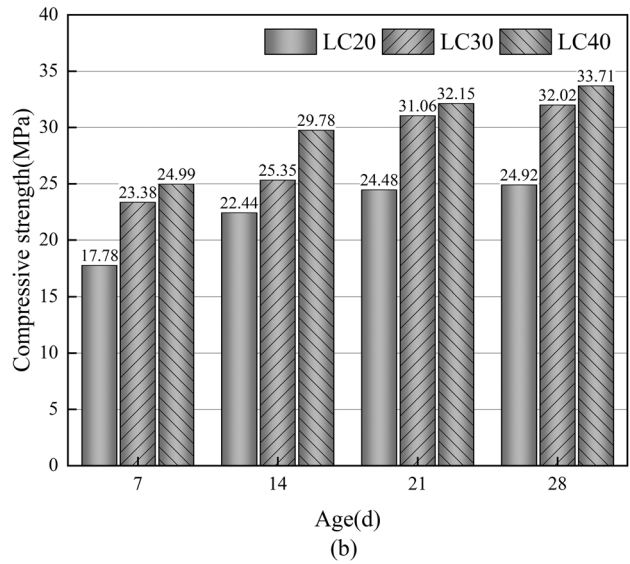


Figure 8: Compressive strength of PAC: (a) different strengths and (b) different curing ages.

$$\log S_{\rm v} = (3 - D) \left(\log \frac{r}{r_{\rm max}} \right), \tag{5}$$

where $S_{\rm v}$ is the cumulative pore volume as a percentage of the total pore volume when the relaxation time is less than the T_2 cutoff value, D is the fractal dimension, r is the arbitrary pore diameter, and $r_{\rm max}$ is the maximum pore diameter in the pore.

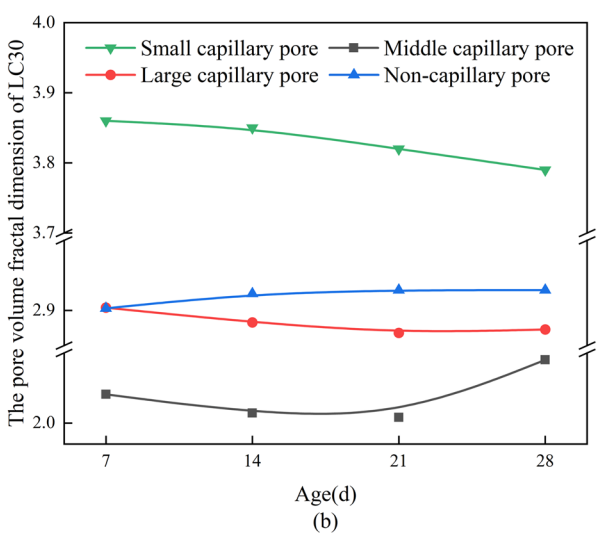
Figure 9 illustrates the variation of the fractal dimension of PAC with the curing age. According to fractal theory [35-37], the fractal dimension of pore surfaces typically falls within the range of 2.000-3.000. If the fractal dimension of pore surfaces in a specific pore size region exceeds this range, it is considered that the region does not exhibit fractal characteristics. By the fitting of NMR data, we discovered that pumice concrete exhibited multiple fractal features. However, the fractal dimension of small capillary pores was consistently found to be greater than 3.000 in the PAC. This finding suggests that PAC does not possess fractal characteristics within the small capillary pore range, which aligns with previous research [38,39]. Other pore volume fractal dimensions for pumice aggregate concrete range from is 2.004 to 2.972. The fractal dimensions of medium and large capillary pores tend to decrease and increase thereafter with an increase in maintenance age. The reason is that the addition of pumice aggregate increases the volume of medium and large capillary pores. Moreover, when the pumice aggregate is incorporated, there are many pores larger than the corresponding fractal pores, enabling the fractal dimension of the corresponding pores to be reduced; the fractal dimensions of medium and large capillary pores gradually refine with an increase in maintenance age and the fractal dimension gradually

increases. The fractal dimension of non-capillary pores, on the other hand, shows a positive trend in relation to the age of maintenance. The fractal dimension change of non-capillary pores is influenced by the pumice aggregate, which provides nucleation sites for the hydration reaction. Moreover, the hydration products refine the non-capillary pores in PAC, increasing the internal pore complexity of PAC. Thus, the fractal dimension of non-capillary pores increases with an increase in the curing age.

Pores of different sizes and shapes are produced in PAC, and pore structure changes with increasing curing age; a change in the pore structure will determine the change in its compressive strength. The study of the pore structure generated by aggregate accumulation has matured [40–42], and will not be elaborated considerably in this study. We will focus on the effect of pore structure on the compressive strength of PAC as influenced by the variation of pore space in the pumice aggregate. By the pore characteristic analysis of PAC, the evolution of the pore characteristics of PAC can be simplified, as shown in Figure 10.

Pumice aggregates have well-defined pore structure characteristics and high specific surface area, which can provide nucleation sites for cement hydration [43]. First, cement mortar and moisture are able to enter the pores of the pumice aggregate and form a dense mortar paste film on the inner surface of the pores of the pumice aggregate [44]. The pore wall of pumice aggregate is filled and extended to the inside, thereby effectively improving the microstructure of pumice aggregate pores. Second, pumice aggregate acts as an internal water reservoir, and water is able to return from the aggregate during maintenance, which can react with the cement particles inside the pores of the

DE GRUYTER



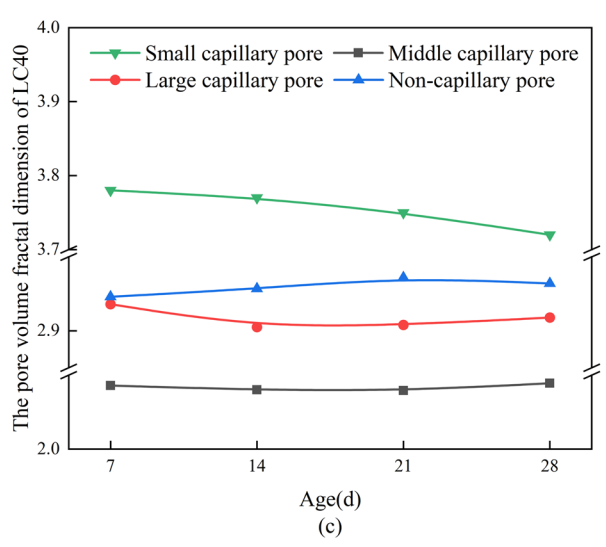


Figure 9: Fractal dimension of PAC: (a) LC20, (b) LC30, and (c) LC40.

aggregate and increase the hydration of the cement [45]. As the age of maintenance increases, calcium hydroxide crystals (C-H) in the cement paste react volcanically with amorphous SiO₂ in the aggregate [46]. Gradually, there is a strong volcanic ash reaction of the paste film in the pores of pumice aggregates, and the resulting C-S-H gel crystals adhere to the pore walls of pumice aggregates. Owing to the disorderly growth of hydration products, the pores of pumice aggregate become more curved and irregular, and there is a gradual differentiation of the larger pores to the smaller ones, increasing the percentage of medium capillary pores and small capillary pore volume. The filling of hydration products inside the pumice aggregate results in the PAC having a tighter microstructure inside [47], with reduced porosity, better cohesion, and enhanced compressive strength. And some lightweight concrete pore structure changes have similarities with pumice concrete, such as expanded perlite [48] as aggregate for the preparation of concrete, mortar containing perlite has large pores, and expanded perlite has a large water absorption capacity in a high humidity environment, and the phenomenon of water reversion will occur during the curing process to achieve the effect of internal curing, which allows the concrete to enhance the overall strength from the inside. In addition, coral aggregate [49] has a similar surface structure to pumice aggregate because of its porous surface properties, and the hydration products fill in the voids of coral aggregate, which makes the pore size gradually transform into small pores and forms interlock in cement paste matrix, which enhances the compressive strength of coral concrete. By comparing other lightweight aggregates, it is found that pumice concrete has the same evolution mechanism as other porous aggregates. As the curing age increases, the hydration reaction continues, the hydration products on the surface of the pore structure of the pumice aggregate inside the concrete gradually extend to the inside of the pores, and the transition zone of the interface between the pumice aggregate and the cement paste becomes denser, making the concrete gradually stronger.

4 Compressive strength model for PAC based on pore characteristics

4.1 Correlation analysis

To determine the influence of pore structure characteristic parameters of PAC on its compressive strength, compressive

strength was used as the reference sequence, and the porosity and the percentage of each pore size interval as the comparison sequence. Moreover, the correlation between the reference and comparison sequences was obtained using the calculation method of Dunn's correlation (Table 5). Table 5 shows that the correlation of LC20 pore structure parameters on the compressive strength is as follows: percentage of medium capillaries > percentage of small capillaries > percentage of large capillaries > porosity > percentage of non-capillary pore. The LC30 pore structure parameters on the compressive strength are as follows: percentage of large capillaries > percentage of medium capillaries > percentage of small capillaries > porosity > percentage of non-capillary pore. Finally, the LC40 pore structure parameters on the compressive strength are as follows: percentage of large capillaries > percentage of small capillaries > percentage of medium capillaries > porosity > percentage of non-capillary pore. Therefore, the compressive strength is highly correlated with the percentages of small capillary pores, medium pore size, and large pore size and less correlated with the percentage of porosity and non-capillary pores.

4.2 Establishment of the compressive strength prediction model

The gray model can generate a strong regular data series by accumulating randomly generated data, calculating the corresponding parameters using the least-squares method, building the relevant equation model, and predicting the trend of further development. According to the correlation analysis [50], the compressive strength of PAC was found to

be highly correlated with the percentages of small capillary pores, medium capillary pore size, and large capillary pore size. However, the percentage of small capillaries in PAC ranged from 1.98 to 3.51% of the pore volume, thereby having a small effect on the compressive strength [51]. Therefore, the percentage of medium and large capillaries were selected as indicators to establish the GM(1,3) gray models of LC20, LC30, and LC40 strengths to obtain the development pattern of the compressive strength of PAC.

To build a gray system model to perform certain operations on the data series to weaken the randomness and highlight the trend of the data series, various forms of operations are defined first as follows.

Let the original sequence be $X_i^{(0)} = (x_i^{(0)}(1), x_i^{(0)}(2), x_i^{(0)}(3), \dots x_i^{(0)}(n))(i=2,3,\dots,n)$. Its first-order cumulative generation (1-AGO) sequence is defined as $X_i^{(1)} = (x_i^{(1)}(1), x_i^{(1)}(2), x_i^{(1)}(3), \dots x_i^{(1)}(n))(i=2,3,\dots,n)$, of which $x_i^{(1)}(n) = \sum_{i=1}^n x^{(0)}(1)$. The immediate neighboring mean of the sequence $X_1^{(1)}$ generates a sequence of $Z_1^{(1)}$, defined as $Z_1^{(1)} = (z^{(1)}(2), z^{(1)}(3),\dots,z^{(1)}(n))$. Among them, $z^{(1)}(n) = (x^{(1)}(n) + x^{(1)}(n-1))/2$, $z^{(1)}(n)$ is the corresponding first-order cumulative generated value of the original sequence $Z_1^{(0)}$.

According to the preceding definition, let $x_1^{(0)}$ be the compressive strength of PAC and $x_i^{(0)}(i=2,3)$ be the percentages of the medium and large capillary pores. The GM (1, N) model is established as follows:

$$x_1^{(0)}(k) = -az_1^{(1)}(k) + b_2x_2^{(1)}(k) + b_3x_3^{(1)}(k) + \dots + b_Nx_N^{(1)}(k), \quad (6)$$

where the parameters are defined as $\hat{a} = [b_2, b_3, a]^T$, and the model coefficient vector equation $\hat{a} = (B^T B)^{-1} B^T Y$ is obtained according to the least-squares estimation:

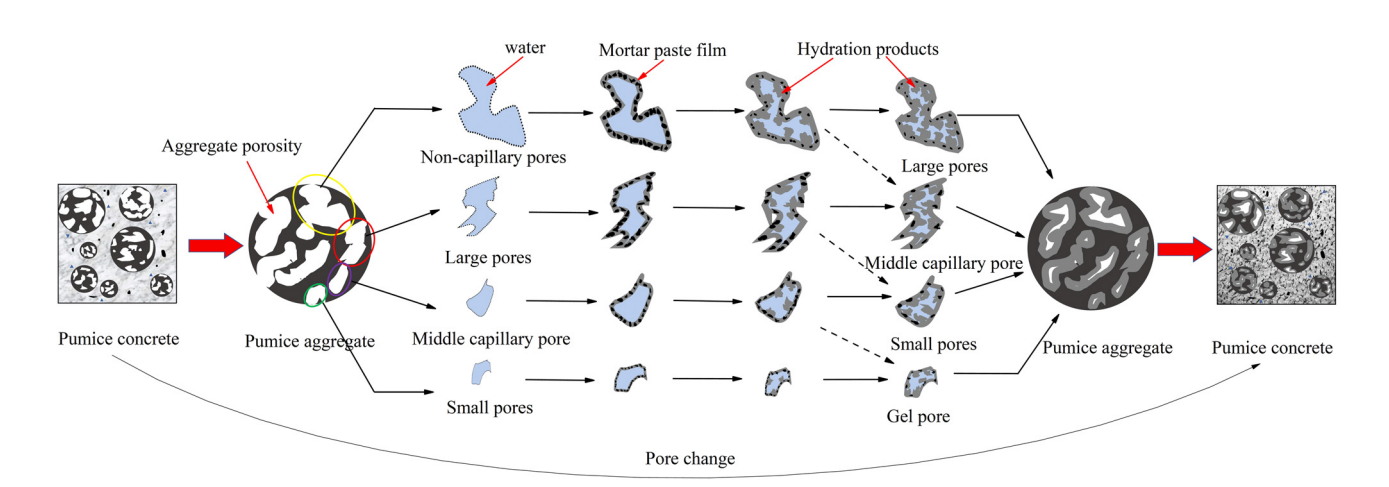


Figure 10: Pore evolution diagram of pumice aggregate.

$$B = \begin{bmatrix} -z_1^{(1)}(2) & x_2^{(1)}(2) & \cdots & x_n^{(1)}(2) \\ -z_1^{(1)}(3) & x_2^{(1)}(3) & \cdots & x_n^{(1)}(3) \\ \vdots & \vdots & \ddots & \vdots \\ -z_1^{(1)}(n) & x_2^{(1)}(n) & \cdots & x_n^{(1)}(n) \end{bmatrix}, Y = \begin{bmatrix} x_1^{(0)}(2) \\ x_1^{(0)}(3) \\ \vdots \\ x_1^{(0)}(n) \end{bmatrix}. \tag{7}$$

The test data were substituted into the preceding equations to obtain three PAC compressive strength prediction models:

$$LC20 x_1^{(0)}(k) = -1.1965 z_1^{(1)}(k) + 0.0021 x_2^{(1)} + 1.3242 x_3^{(1)},$$
 (8)

LC30
$$x_1^{(0)}(k) = -1.3537z_1^{(1)}(k) + 0.1565x_2^{(1)} + 1.8538x_3^{(1)},$$
 (9)

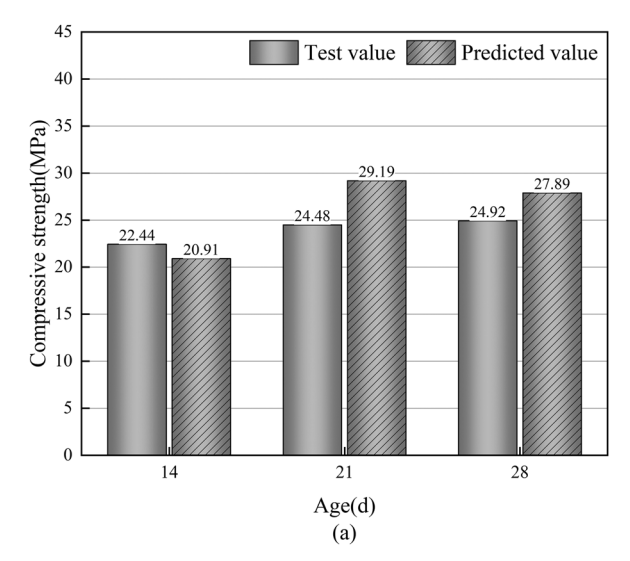
LC40
$$x_1^{(0)}(k) = -1.1492 z_1^{(1)}(k) + 0.9704 x_2^{(1)} - 0.9231 x_3^{(1)}$$
. (10)

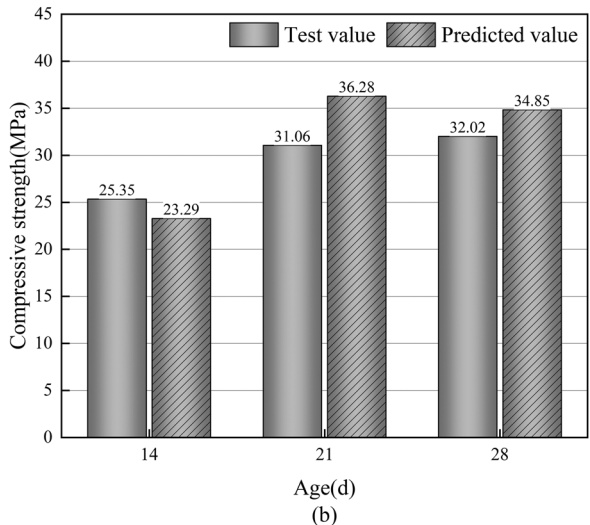
4.3 Validation of the model

Figure 11 shows the predicted values of the GM(1,3) prediction model, experimental values of the tests, and relative errors of the two. The compressive strength obtained from the PAC compressive strength prediction model has minimal error compared with the test values. The relative errors of PAC were in the range 6.40–19.89%, with average errors of 12.65, 11.24, and 13.26% (*i.e.*, below 20%). To ensure the applicability of the developed model, NMR data measured from ordinary concrete in the literature [52] was substituted into the model. For the LC20 model, the relative errors were obtained as 18.04, 2.44, and 11.42%. For the LC40 model, the relative errors were 5.00, 44.81, and

Table 5: Correlation analysis

Sample	Influential factors	Correlation
LC20	Porosity	0.5757
	Small capillary pores	0.6702
	Middle capillary pores	0.7189
	Large capillary pores	0.6403
	Non-capillary pores	0.5753
LC30	Porosity	0.5849
	Small capillary pores	0.6743
	Middle capillary pores	0.6929
	Large capillary pores	0.8699
	Non-capillary pores	0.5764
LC40	Porosity	0.5759
	Small capillary pores	0.6545
	Middle capillary pores	0.6532
	Large capillary pores	0.7949
	Non-capillary pores	0.5548





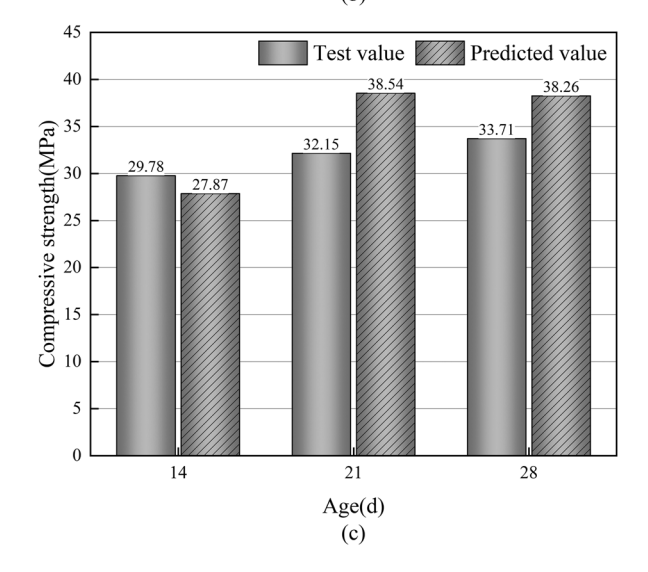


Figure 11: Simulation value, and test value, (a) LC20, (b) LC30, and (c) LC40.

14.54%. Additionally, by substituting the NMR data of wind-deposited sand concrete [53] into the present model, the relative errors for the LC40 model were obtained as 15.25, 2.50, and 7.33%. These results indicate that when using the compressive strength model developed for PAC to predict the compressive strength of other concrete types, the relative errors between the obtained test values and simulated values are small. This demonstrates the high accuracy of the GM (1,3) model established in this study for predicting the compressive strength of PAC, considering both the percentage of the medium pore size and that of the large pore size.

5 Conclusions

In this study, we investigate the microstructure and mechanical properties evolution of PAC at different curing ages. The following conclusions were drawn:

- 1) The pumice aggregate porosity ranged between 17.92 and 45.73%, and the pore size distribution ranged between 1 and 100,000 μm , showing a rich pore structure of pumice aggregate. The pumice concrete porosity ranged from 2.11 to 5.68%, and the pore size distribution ranged from 0.046 to 1,659 μm , showing a three-peaked structure.
- 2) The pore fractal dimension of PAC ranged from 2.004 to 3.861. The fractal dimension of small capillaries is between 3.724 and 3.861 and does not have fractal characteristics. The fractal dimension of medium capillaries is between 2.004 and 2.089, and the pore surface is smooth and gentle; the fractal dimension of large capillaries and non-capillaries is between 2.808 and 2.972, and the pore surface is rough.
- 3) The enhancement of the compressive strength of PAC is influenced by changes in the pore structure of pumice aggregates. The rich pore structure of pumice aggregate can provide nucleation sites for cement hydration. With the growth of age, the C-S-H gel crystals produced by hydration can grow disorderly inside the pores of pumice aggregate and fill in the inside of the pores of pumice aggregate. The concrete is more compact inside and the compressive strength is gradually enhanced.
- 4) Based on the pore structure characteristics of PAC, a GM(1,3) prediction model with a medium and large capillary pore size ratio was established to predict the compressive strength and the relative errors between the predicted and tested values of the model were in the range of 6.40–19.89%. The accuracy of the model

was also verified in plain concrete and wind-cured concrete, and the average relative errors ranged from 8.36 to 21.45%, and the prediction of compressive strength using the model is feasible.

Acknowledgments: The authors would like to thank the researchers at the School of Civil Engineering, Inner Mongolia University of Technology, the School of Materials Science and Engineering, Inner Mongolia University of Technology, and the Key Laboratory of Civil Structures and Mechanics, Inner Mongolia University of Technology, who supported the process required to carry out the project.

Funding information: This study was supported by the Central Guidance on Local Science and Technology Development Fund (Grant No. 2021ZY0024), Natural Science Foundation of Inner Mongolia Autonomous Region (Grant No. 2022MS05034), the Science and Technology Project of Inner Mongolia (Grant No. 2022YFHH0153), Basic Scientific Research Expenses Program of Universities directly under Inner Mongolia Autonomous Region (Grant No. JY20220005), and National Natural Science Foundation of China (Grant No. 52069024).

Author contributions: Xiaoxiao Wang: investigation, formal analysis, writing – original draft, and funding acquisition; Dexi Li: data curation and writing – original draft; Ru Bai: supervision and writing – review and editing; Shuguang Liu: conceptualization and funding acquisition; Changwang Yan: resources and supervision; Ju Zhang: investigation and methodology. All authors have accepted responsibility for the entire content of this manuscript and approved its submission.

Conflict of interest: The authors state no conflict of interest.

Data availability statement: The datasets generated during and/or analysed during the current study are available from the corresponding author on reasonable request.

References

- [1] Shaikh, F. A., P. Nath A. Hosan, M. John, and W. K. Biswas. Sustainability assessment of recycled aggregates concrete mixes containing industrial by-products. *Materials Today Sustainability*, Vol. 5, 2019, id. 100013.
- [2] Łagosz, A., D. Olszowski, W. Pichór, and Ł. Kotwica. Quantitative determination of processed waste expanded perlite performance

- as a supplementary cementitious material in low emission blended cement composites. Journal of Building Engineering, Vol. 40, 2021, id. 102335.
- [31 Soykan, O., Ö. Cengiz, and Ö. Cenk. Arduvaz ve Andezit'in Beton Agregası Olarak Kulanılabilirliğinin Araştırılması. Süleyman Demirel Üniversitesi Fen Bilimleri Enstitüsü Dergisi, Vol. 19, No. 1, 2015,
- Wang, F., Y. Sun, X. Xue, N. Wang, J. Zhou, and J. Hua. Mechanical properties of modified coral aggregate seawater sea-sand concrete: Experimental study and constitutive model. Case Studies in Construction Materials, Vol. 18, 2023, id. e02095.
- Cavaleri, L., N. Miraglia, and M. Papia. Pumice concrete for structural wall panels. Engineering Structures, Vol. 25, No. 1, 2003, pp. 115-125.
- [6] Mo, K. H., T. C. Ling, U. J. Alengaram, S. Yap, and C. W. Yuen. Overview of supplementary cementitious materials usage in lightweight aggregate concrete. Construction and Building Materials, Vol. 139, 2017, pp. 403-418.
- Algarni, A. S. A comprehensive review on properties of sustainable concrete using volcanic pumice powder ash as a supplementary cementitious material. Construction and Building Materials, Vol. 323, 2022, id. 126533.
- Shafiq, M. S., F. A. Khan, Y. I. Badrashi, F. A. Khan, M. Fahim, A. Abbas, et al. Evaluation of Mechanical Properties of Lightweight Concrete with Pumice Aggregate. Advances in Science and Technology. Research Journal, Vol. 152, 2021, pp. 30-38.
- [9] Hassanpour, M., Shafigh, and H. B. Mahmud. Lightweight aggregate concrete fiber reinforcement-A review. Construction and Building Materials, Vol. 37, 2012, pp. 452-461.
- [10] Tanyıldızı, M. and İ. Gökal. Utilization of pumice as aggregate in the concrete: A state of art. Construction and Building Materials, Vol. 377,
- [11] Cabrera-Luna, K., E. E. Maldonado-Bandala, D. Nieves-Mendoza, P. Castro-Borges, P. Perez-Cortes, and J. E. García. Supersulfated cements based on pumice with quicklime, anhydrite and hemihydrate: Characterization and environmental impact. Cement and Concrete Composites, Vol. 124, 2021, id. 104236.
- [12] Kashyap, A. M. N. and G. Sasikala. An experimental study on compressive strength of steel fibre reinforced light weight aggregate (Pumice Stone) concrete. International Journal of Engineering Research and Development, Vol. 9, No. 12, 2014, pp. 21-25.
- [13] Liu, K., R. Yu, Z. Shui, X. Li, C. Guo, B. Yu, et al. Optimization of autogenous shrinkage and microstructure for Ultra-High Performance Concrete (UHPC) based on appropriate application of porous pumice. Construction and Building Materials, Vol. 214, 2019, pp. 369-381.
- [14] Ghabezloo, S., J. Sulem, S. Guédon, F. Martineau, and J. Saint-Marc. Poromechanical behaviour of hardened cement paste under isotropic loading. Cement and Concrete Research, Vol. 38, No. 12, 2008, pp. 1424-1437.
- Erenson, C. and M. Kalkan. An investigation of the void structure of [15] lightweight concrete containing waste undersize pumice additive using nondestructive methods. Russian Journal of Nondestructive Testing, Vol. 57, No. 8, 2021, pp. 679-691.
- [16] Liu, C., H. Cen, X. Wang, C. Yan, S. Liu, and J. Zhang. Parallel bar compressive strength model for pumice concrete considering frost-heave stress. Journal of Materials in Civil Engineering, Vol. 35, No. 3, 2023, id. 04022481.
- [17] Gao, H., X. Zhang, and Y. Zhang. Effect of the entrained air void on strength and interfacial transition zone of air-entrained mortar.

- Journal of Wuhan University of Technology-Mater. Science Education, Vol. 30, No. 5, 2015, pp. 1020-1028.
- [18] Nasharuddin, R., G. Luo, N. Robinson, A. Fourie, M. L. Johns, and E. O. Fridjonsson. Understanding the microstructural evolution of hypersaline cemented paste backfill with low-field NMR relaxation. Cement and Concrete Research, Vol. 147, 2021, id. 106516.
- Santos, A. R., M. do Rosário Veiga, A. S. Silva, and J. de Brito. Microstructure as a critical factor of cement mortars' behaviour: The effect of aggregates' properties. Cement and Concrete Composites, Vol. 111, 2020, id. 103628.
- [20] Liu, Q., X. Shen, L. Wei, R. Dong, and H. Xue. Grey model research based on the pore structure fractal and strength of NMR aeolian sand lightweight aggregate concrete. Jom, Vol. 721, 2020, pp. 536-543.
- [21] Hossain, K. M. A. Potential use of volcanic pumice as a construction material. Journal of Materials in civil Engineering, Vol. 166, 2004, pp. 573-577.
- [22] Wang, X., Y. Wu, X. Shen, H. Wang, S. Liu, and C. Yan. An experimental study of a freeze-thaw damage model of natural pumice concrete. Powder Technology, Vol. 339, 2018, pp. 651-658.
- [23] Zhang, C., J. Fu, W. Song, C. Du, and H. Fu. High-volume ultrafine fly ash-cement slurry mechanical properties and strength development model establishment. Construction and Building Materials, Vol. 277, 2021, id. 122350.
- [24] Wang, X., C. Liu, S. Liu, C. Yan, J. Zhang, and H. Li. Compressive strength of pile foundation concrete in permafrost environment in China. Construction and Building Materials, Vol. 247, 2020, id. 118431.
- [25] Li, Y. D., C. Yang, and S. Feng. Method of studying pore diameter distribution of shale by nuclear magnetic resonance. Geology. Review, Vol. 63, 2017, pp. 119-120.
- [26] Li, H., J. Zhu, and H. Guo. Methods for calculating pore radius distribution in rock from NMR T2 spectra. Chinese Journal of Magnetic Resonance, Vol. 25, 2008, pp. 273-280.
- [27] Kumar, R. and B. Bhattacharjee. Porosity, pore size distribution and in situ strength of concrete. Cement and Concrete Research, Vol. 331, 2003, pp. 155-164.
- [28] Paul, A., S. Murgadas, J. Delpiano, P. A. Moreno-Casas, M. Walczak, and M. Lopez. The role of moisture transport mechanisms on the performance of lightweight aggregates in internal curing. Construction and Building Materials, Vol. 268, 2021, id. 121191.
- [29] Karakaş, H., S. İlkentapar, U. Durak, E. Örklemez, S. Özuzun, O. Karahan, et al. Properties of fly ash-based lightweight-geopolymer mortars containing perlite aggregates: Mechanical, microstructure, and thermal conductivity coefficient. Construction and Building Materials, Vol. 362, 2023, id. 129717.
- Erdem, S., A. R. Dawson, and N. H. Thom. Impact load-induced micro-structural damage and micro-structure associated mechanical response of concrete made with different surface roughness and porosity aggregates. Cement and Concrete Research, Vol. 422, 2012, pp. 291-305.
- Zhang, X., K. Wei, D. Li, Y. Zhou, and W. Liang. Characterization of mechanical properties and microstructure of silica mortar and coral mortar based on nuclear magnetic resonance technology. Materials Today Communications, Vol. 33, 2022, id. 104909.
- [32] Wang, L., X. Zeng, H. Yang, X. Lv, F. Guo, Y. Shi, et al. Investigation and application of fractal theory in cement-based materials: A review. Fractal and Fractional, Vol. 54, 2021, id. 247.
- [33] Pandey, S. and R. L. Sharma. The influence of mineral additives on the strength and porosity of OPC mortar. Cement and Concrete Research, Vol. 301, 2000, pp. 19-23.

- [34] Zhao, Y., G. Zhu, Y. Dong, N. N. Danesh, Z. Chen, and T. Zhang. Comparison of low-field NMR and microfocus X-ray computed tomography in fractal characterization of pores in artificial cores. *Fuel*, Vol. 210, 2017, pp. 217–226.
- [35] Meng, Q., Q. Qin, H. Yang, H. Zhou, K. Wu, and L. Wang. Fractal characteristics of the pore structure of coral powder–cement slurry under different fractal models. *Fractal and Fractional*, Vol. 6, No. 3, 2022. id. 145.
- [36] Peng, Y., S. Tang, J. Huang, C. Tang, L. Wang, and Y. Liu. Fractal analysis on pore structure and modeling of hydration of magnesium phosphate cement paste. *Fractal and Fractional*, Vol. 6, No. 6, 2022, id. 337.
- [37] Huang, J., W. Li, D. Huang, L. Wang, E. Chen, C. Wu, et al. Fractal analysis on pore structure and hydration of magnesium oxysulfate cements by first principle, thermodynamic and microstructurebased methods. Fractal and Fractional, Vol. 5, No. 4, 2021, id. 164.
- [38] Liu, L., Z. Fang, C. Qi, B. Zhang, L. Guo, and K. I. Song. Experimental investigation on the relationship between pore characteristics and unconfined compressive strength of cemented paste backfill. *Construction and Building Materials*, Vol. 179, 2018, pp. 254–264.
- [39] Ning, L., Y. Zhao, J. Bi, C. Wang, M. Shen, and Y. Li. Effect of aggregate size on water distribution and pore fractal characteristics during hydration of cement mortar based on low-field NMR technology. Construction and Building Materials, Vol. 389, 2023, id. 131670.
- [40] Rashad, A. M. A short manual on natural pumice as a lightweight aggregate. *Journal of Building Engineering*, Vol. 25, 2019, id. 100802.
- [41] Jennings, H. M., J. W. Bullard, J. J. Thomas, J. E. Andrade, J. J. Chen, and G. W. Scherer. Characterization and modeling of pores and surfaces in cement paste: correlations to processing and properties. *Journal of Advanced Concrete Technology*, Vol. 61, 2008, pp. 5–29.
- [42] Chen, X. and S. Wu. Influence of water-to-cement ratio and curing period on pore structure of cement mortar. *Construction and Building Materials*, Vol. 38, 2013, pp. 804–812.
- [43] Seraj, S., R. Cano, R. D. Ferron, and M. C. Juenger. The role of particle size on the performance of pumice as a supplementary cementitious material. *Cement and Concrete Composites*, Vol. 80, 2017, pp. 135–142.

- [44] Li, L. G., J. J. Feng, Z. C. Lu, H. Z. Xie, B. F. Xiao, A. K. H. Kwan, et al. Effects of aggregate bulking and film thicknesses on water permeability and strength of pervious concrete. *Powder Technology*, Vol. 396, 2022, pp. 743–753.
- [45] Weber, S. and H. W. Reinhardt. A new generation of high performance concrete: concrete with autogenous curing. *Advanced cement based materials*, Vol. 62, 1997, pp. 59–68.
- [46] Liu, C., W. Zhang, H. Liu, C. Zhu, Y. Wu, C. He, et al. Recycled aggregate concrete with the incorporation of rice husk ash: mechanical properties and microstructure. *Construction and Building Materials*, Vol. 351, 2022, id. 128934.
- [47] Pinarci, İ. and Y. Kocak. Hydration mechanisms and mechanical properties of pumice substituted cementitious binder. *Construction and Building Materials*, Vol. 335, 2022, id. 127528.
- [48] Xiong, H., K. Yuan, J. Xu, and M. Wen. Pore structure, adsorption, and water absorption of expanded perlite mortar in external thermal insulation composite system during aging. *Cement and Concrete Composites*, Vol. 116, 2021, id. 103900.
- [49] Wang, Q., P. Li, Y. Tian, W. Chen, and C. Su. Mechanical properties and microstructure of Portland cement concrete prepared with coral reef sand. *Journal of Wuhan University of Technology-Material Science Ed*, Vol. 315, 2016, pp. 996–1001.
- [50] Wang, X., R. Feng, J. Li, S. Liu, and C. Yan, Wear characteristics and degradation mechanism of natural pumice concrete under ice friction during ice flood season, *Construction and Building Materials*, Vol. 341, 2022, id. 127742.
- [51] Zhang, S., Z. Li, B. Ghiassi, S. Yin, and G. Ye. Fracture properties and microstructure formation of hardened alkali-activated slag/fly ash pastes. *Cement and Concrete Research*, Vol. 144, 2021, id. 106447.
- [52] Lei, S. Correlation analysis of concrete porous structure and compressive strength based on age variation. *China Building Materials Technology*, Vol. 29, No. 6, 2020, pp. 63–66.
- [53] Xiangdong, S. and D. Ruixin. Grey entropy analysis on effect of pore structure on compressive strength of aeolian sand concrete. *Transactions of the Chinese Society of Agricultural Engineering*, Vol. 35, No. 10, 2019, pp. 108–114.